Hindawi
Geofluids
Volume 2022, Article ID 9726379, 17 pages
https://doi.org/10.1155/2022/9726379

Research Article

Study on Gas Migration Law of Mining Coal Seam under the Influence of Normal Fault

Xiangtao Kang[1,2] **Meng Tang**[1] **Mingquan Jiang**[1] **Cunliu Zhou**[1] **Jinguo Hu**[1] **Jiachi Ren**[1] **and Bozhi Deng**[3]

[1]*Mining College, Guizhou University, Guiyang 550025, China*
[2]*Key Laboratory of Safe and Effective Coal Mining (Anhui University of Science and Technology), Huainan 232000, China*
[3]*State Key Lab Coal Mine Disaster Dynamics & Control, Chongqing University, Chongqing 400030, China*

Correspondence should be addressed to Meng Tang; tangmenguu@163.com

Received 30 June 2022; Revised 5 August 2022; Accepted 13 August 2022; Published 5 September 2022

Academic Editor: Liang Xin

In order to study the coupling law of mining and gas migration in close coal seams in fault structure area, taking the coal mining face in Guizhou as the research background, the development of mining fracture field and gas migration law of No. 5 coal seam and No. 9 coal seam were studied. Based on the development of mining-induced fracture field in coal seam, the fracture distribution was binarized and quantitatively analyzed by using fractal dimension, and the gas migration law of mining-induced fractures in No. 5 coal seam and No. 9 coal seam was simulated and studied. The results show that under the condition of U-shaped ventilation, the gas accumulates seriously in the upper corner of the mining fracture field, and the gas generally floats and accumulates to the separated layer development area of the overlying strata. Due to the existence of faults, even if the mining-induced fracture field in goaf of No. 9 coal seam is within the mining-induced pressure relief range of No. 5 coal seam, the gas concentration in the mining-induced fracture field is still high, and the variation gradient of gas concentration is large. The gas will circulate actively and accumulate easily near the fault structure, and the gas concentration at the high level of the fault is slightly higher than that at the low level. The research results can provide some reference for the mining of close coal seams in the fault structure area, the comprehensive prevention and control of gas, and the safe and efficient production of coal mines.

1. Introduction

China is rich in coal resources. The proportion of coal in China's primary energy consumption structure will remain at about 50% in 2050. Therefore, coal is still the most important energy resource in China for a long time [1]. However, after coal forming in coal-bearing strata in China, under several severe geological tectonic movements, coal and rock strata continue to suffer compression, shear, and other damage, resulting in complex geological structures in many coalfields in China and many fault structures [2, 3]. Faults destroy the continuity of coal seams, which is an important factor causing frequent accidents in coal mines. In particular, the occurrence of coal and gas outburst accidents is closely related to fault structures [4–7]. According to relevant statistical data, most of the prominent accidents in Pingdingshan mining area, Jiaozuo mining area, and Huainan mining area in China are related to fault-based structures [6–11]. 134 coal and gas outburst accidents occurred in the eastern mining area of Pingdingshan; most of them occurred in the vicinity of fault structural belt, especially the small fault which has obvious influence on gas outburst accidents, and tectonic coal widely developed in the outburst area [6]; Daping coal mine gas accident occurred near the reverse fault, and outburst accident caused 1894 tons of coal into the working face, resulting in 148 deaths [7]. Production practice also shows that the average intensity and frequency of outburst accidents in areas with fault geological structure are far greater than those in areas without fault structure [11]. It can be seen that the fault area is an important area of coal mine disasters, and the existence of faults seriously threatens the safe mining of coal seams.

Microfractures in the coal seam reservoir and the macrofractures caused by geological evolution lead to gas and water seepage and leakage in the reservoir [12]. Coal seam will produce a large number of joints and cracks in the mining process. Mining cracks are the main channel of gas migration. Finding out the migration law of gas undermining conditions is conducive to putting forward targeted gas prevention measures. Zhu et al. [13] believe that the existence of faults will significantly affect the characteristics of gas migration, and different fault types can play a role in sealing or diversion of gas migration. Bradley [14] studied the role of normal faults in gas flow by using the seismic reflection data in the southern Taranaki Basin, New Zealand. Many scholars have also conducted a lot of research on the gas migration law undermining conditions. Li et al. [15, 16] used Kozery theory to study the correlation between rock expansion coefficient and permeability, defined the goaf as the seepage of heterogeneous variable permeability coefficient, and obtained the gas diffusion equation in goaf. On the basis of analyzing the characteristics of goaf, Liu et al. [17] proposed the control equations reflecting the characteristics of gas migration in fully mechanized mining face. The Boltzmann method (LBM) was used to simulate the gas migration in goaf of fully mechanized caving face, and the gas migration was intuitively simulated and analyzed. Liu et al. [18] constructed the seepage model of goaf by combining seepage theory, mechanical theory, and numerical simulation and obtained the distribution law of gas concentration and seepage field in goaf. Starting from the relevant physical principles, Zhao et al. [19] analyzed the effects of medium deformation, two-phase flow, and mass/gas transfer on the transport process of methane gas in porous media. Li et al. [20, 21] studied the stress distribution characteristics of coal seam floor and the variation law of pressure relief gas seepage velocity during working face advancing through experiments and proposed that the "elliptical throwing zone" was used to characterize the fracture development morphology of mining rock. At the same time, the "pressure relief gas seepage-floating-diffusion model" based on "elliptical throwing zone" was established to describe the pressure relief gas migration law of mining rock. Zhu et al. [22] based on the physical coupling process of coal and rock deformation and pressure relief gas migration introduced the coupling variables in the control equation of coal and rock seepage field and gas seepage field and established a new solid-gas coupling mathematical model of coal mining rock deformation and pressure relief gas flow coupling, which laid a theoretical foundation for the numerical calculation of coal mining rock deformation and gas migration law in outburst coal seam group. Gao et al. [23] used FLAC^{3D} to study the stress of stope and crack propagation according to the stress state of coal body in front of the work and simulated and analyzed the gas migration law under the influence of mining through the self-established solid-gas coupling constitutive model considering gas pressure and gas adsorption. Yang et al. and Cheng et al. [24, 25] studied the fracture development characteristics of overlying strata under the influence of mining and simulated and analyzed the gas migration law in the fracture area. In [26] in view of the technical problems of safe mining caused by high gas and low permeability of coal seams in mining areas in China, based on the theory of pressure relief gas drainage, the pressure relief gas drainage technology and coal and gas comining technology system were established. Cao et al. [27] studied the extraction of fractured gas based on the simulation analysis of gas migration in mining fractures, which provided an effective reference for gas control in the field.

Guizhou Province in China is located in the transition zone of the Yangtze block, Jiangnan and Youjiang orogenic belt. Due to the long-term collision and compression of the surrounding geological plates, the structure is complex, and different combinations of folds, faults, and ductile shear zones are developed [28]. The strong tectonic deformation makes Guizhou form its own unique mountainous terrain and geomorphology conditions. Fault, high gas, close coal seam group, and low permeability are the common characteristics of coal seam mining in Guizhou. Most of the mining areas in Guizhou are mountainous terrain, with developed fault structures and complex geological conditions. Most of the coal mines are coal and gas outburst mines, and gas control is difficult and accidents occur frequently. Gas occurrence and migration law is the basis of gas disaster prevention and control. Under the condition of fault influence and close outburst coal seam mining, the gas migration law of mining fracture field is more complex, and the gas dynamic disaster under fault structure poses a serious threat to the safe mining of Guizhou mines. Therefore, in view of the complex geological conditions of multifault structures and most of them are close coal seams in Guizhou coalfield, it is of great significance to carry out the research on the gas migration law of mining-induced coal seams under the influence of faults, which not only plays an important role in exploring the disaster-causing mechanism of gas dynamic disasters under fault structures but also has great significance for the coal seam mining near faults, gas prevention and control, and safe and efficient production of coal mines. The research results can provide reference for safe mining and gas comprehensive prevention of close coal seams in fault area.

2. Development Law of Mining Fracture Field under Normal Fault Condition

2.1. Project Profile. A mine in Guizhou is located in Shuicheng mining area with developed faults and folds. The geological structure of the mine is complex, mainly in normal faults, and the gas emission is large, which is a high-gas mine. No. 5 coal seam is located in the upper part of No. 9 coal seam about 40 m, and No. 5 coal seam has been mined; there is no fault development in the mining process, and No. 9 coal seam is being mined. The coal seam comprehensive histogram is shown in Figure 1. The No. 9 coal seam is mainly mined in 210911 working face. The dip angle of No. 9 coal seam is 20~24°, generally 20°, and the thickness of coal seam is 1.15~1.75 m. It contains one to two layers of gangue, which is a complex structure coal seam. Coal seam original gas content 8.462 m^3/t, gas pressure1.4 MPa, belongs to coal and gas outburst coal seam. According to

No.	Lithologic characters	Rodman-shaped	Thickness (m)
1	Siltstone		13~27
2	Fine sandstone		15.5~23
3	Muddy mudstone		10.5~18.5
4	Sandy mudstone		1.5~4.9
5	No. 5 coal seam		2.6
6	Muddy mudstone		2.6~5.8
7	Fine sandstone		4.3~7.5
8	Sandy mudstone		3.7~6.9
9	Siltstone		11~15.5
10	Fine sandstone		2.4~5.3
11	No. 9 coal seam		1.15~1.75
12	Siltstone		1.5~3.4
13	Fine sandstone		1.0~2.7
14			10.5~17.5
15	Muddy mudstone		4.4~7.6
16	No. 12 coal seam		2.4~2.9
17	Mudstone		2.7~13
18	Muddy mudstone		4.6~35

Figure 1: Comprehensive coal seam histogram.

the data of 211209 coal mining face, there is a normal fault with a dip angle of 60°, and the fault drop is about 1.5 m.

2.2. Establishment of Numerical Model. Based on the actual situation of 210911 working face in a mine in Guizhou, the size of the numerical model is designed to be 300 m × 200 m (length × width). In order to eliminate the boundary effect, 50 m protective coal pillars are set on the left and right sides of the model, respectively. The model scheme is shown in Figure 2. The simulation excavation of No. 5 and No. 9 two layers of coal is carried out. First, the No. 5 coal seam is excavated, and then, the No. 9 coal seam is excavated. Based on the actual situation in the field, the mining directions of the two layers of coal are from left to right. The No. 9 coal seam is directly mined through the normal fault layer by the upper panel of the coal mining work. Each coal seam is excavated for 10 steps, 20 m each time. The establishment of numerical model and unit block division are shown in Figure 3.

The Mohr-Coulomb elastic-plastic model is used for the constitutive model of coal and rock mass, and the joint surface contact Coulomb slip model is used for each block. The bottom boundary of the model is set as the displacement boundary that limits the vertical displacement, the left and right boundary is set as the displacement boundary that limits the horizontal displacement, and the upper boundary is the free boundary. Considering the actual burial depth of No. 5 coal seam and the integration of some rock strata in the process of model establishment, uniform load is applied to the uppermost part of the model.

2.3. Analysis of Simulation Results

2.3.1. Simulation Excavation Process Analysis of No. 5 Coal Seam. When No. 5 coal seam is excavated 20 m, 40 m, 60 m, 80 m, 100 m, 120 m, 140 m, 160 m, 180 m, and 200 m, respectively, the distribution of mining-induced fractures is shown in Figure 4.

It can be seen from Figures 4(a)–4(j) that although the excavation of No. 5 coal seam will cause compression on the fault at the underlying position, the fault is generally located in the pressure relief area of the underlying strata after the excavation of No. 5 coal seam. It can be seen from the fracture distribution diagram in Figure 4 that although there are some small fractures at the fault, the fault does not slip and dislocate, and the mining of No. 5 coal seam has little effect on the fault. Due to the existence of faults in the underlying position, the stress in the pressure relief zone near the fault after mining in the underlying strata of No. 5 coal seam will appear singular distribution, which greatly affects the distribution law of fracture development in the region. The fractures are relatively developed near the upper plate of the fault, and the fracture development in the lower plate of the fault is not obvious. The fractures near the upper wall of the fault are mainly horizontal fractures, which is not conducive to the migration of gas to the goaf of No. 5 coal seam and is easy to form gas enrichment in the region. Therefore, when No. 9 coal seam advances to the region, it is necessary to strengthen the prevention and control of gas disasters.

2.3.2. Simulation Excavation Process Analysis of No. 9 Coal Seam. The distribution of mining-induced fractures in No. 9 coal seam is shown in Figure 5 when excavating 20 m, 40 m, 60 m, 80 m, 100 m, 120 m, 140 m, 160 m, 180 m, and 200 m, respectively.

From Figures 5(a)–5(j), it can be seen that the mining of No. 9 coal seam will produce a large number of new mining fractures, and with the continuous progress of No. 9 coal seam mining, the fracture again experienced the development process of development-expansion-compaction. Before passing through the fault, the fault is less affected by mining, and the mining cracks are relatively sparse. The cracks are mainly concentrated in the coal strata of the upper wall of the fault, and there is a certain amount of microthrough cracks in the lower wall of the fault. With the increase of excavation distance, after 40 m, affected by repeated disturbance, the overlying strata collapse violently, and a large range of cracks occur periodic closure and compaction. With the excavation gradually close to the fault, the number of

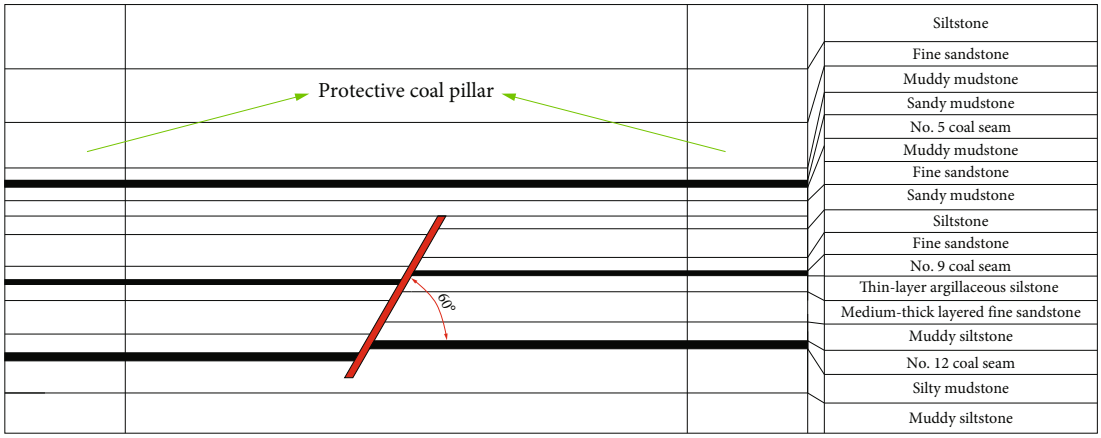

Figure 2: Model solution design.

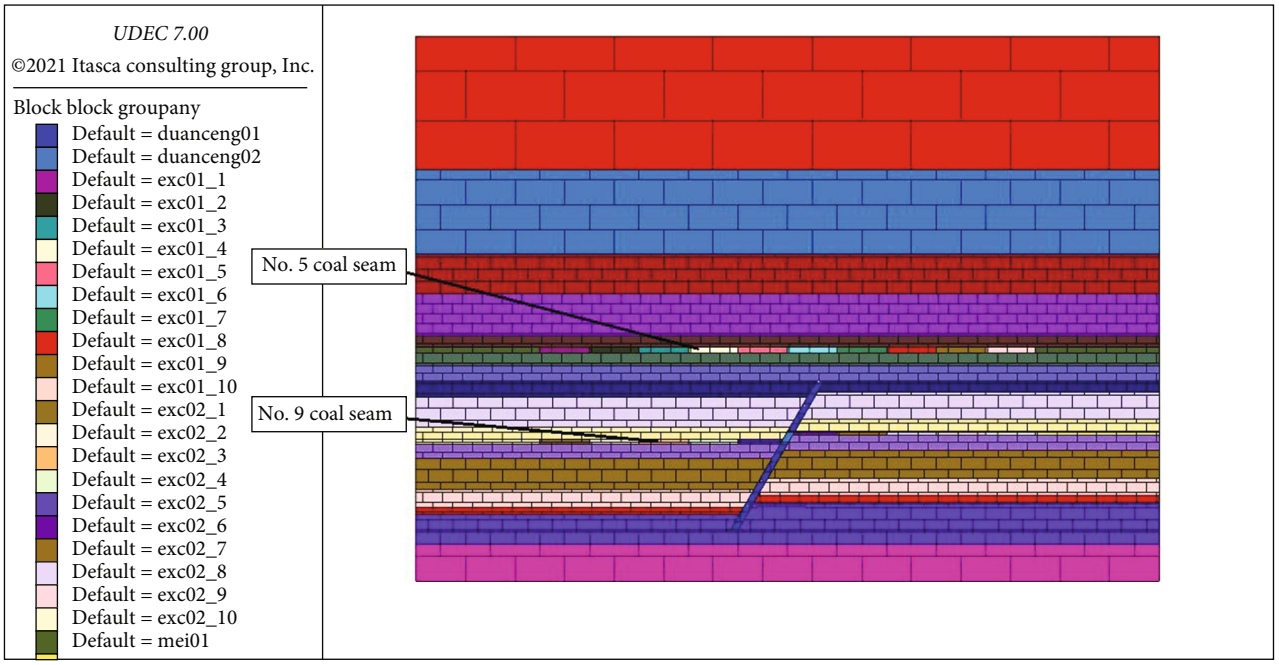

Figure 3: Model block and cell division diagram.

fractures near the fault increases significantly, and there are more broken fractures in the lower plate of the fault, and the development of mining fractures is gradually dense. The mining fractures in the upper plate face develop along the top of the fault to the lower plate. After passing through the fault, the mining-induced fractures are closed and compacted quickly with the periodic weighting and the influence of the self-weight of the upper strata. After gradually moving away from the fault, the change of mining-induced fractures tends to be stable.

2.4. Fractal Study of Mining Fracture. The spatial and temporal distribution characteristics of the development of the mining-induced fracture field in the overlying strata largely determine the strike and occurrence characteristics of the coal seam gas migration. The mining-induced failure process of the overlying strata is an evolution process from bottom to top, from order to disorder. In particular, under the influence of periodic weighting and repeated disturbance, this evolution process is bound to be more complex, and the evolution of the mining-induced fracture field has complex nonlinear characteristics. Yu et al. [29] found that the fracture network formed by rock mining has good statistical self-similar fractal characteristics and proposed using fractal dimension to characterize the degree of fracture of rock mining [30]. Therefore, in recent years, many scholars have used fractal theory to quantify mining-induced fractures under different mining conditions and achieved good results [31,

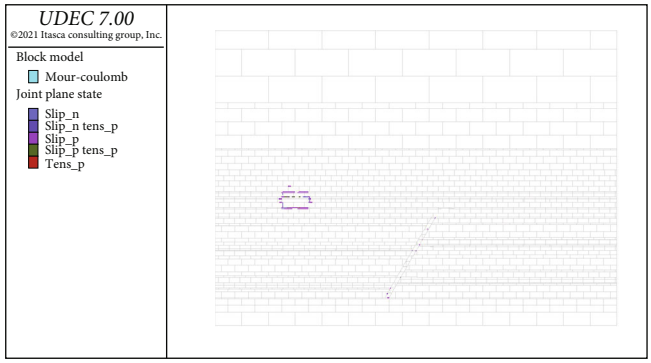

(a) Excavation 20 m

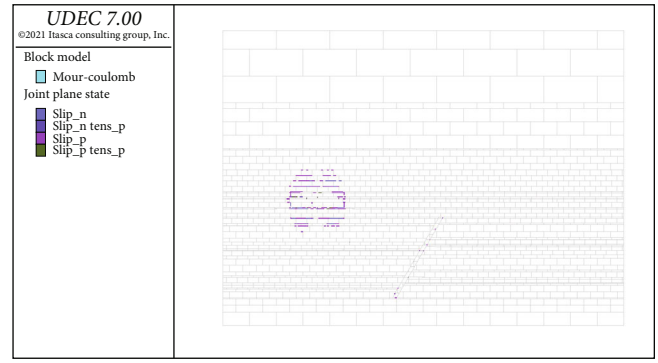

(b) Excavation 40 m

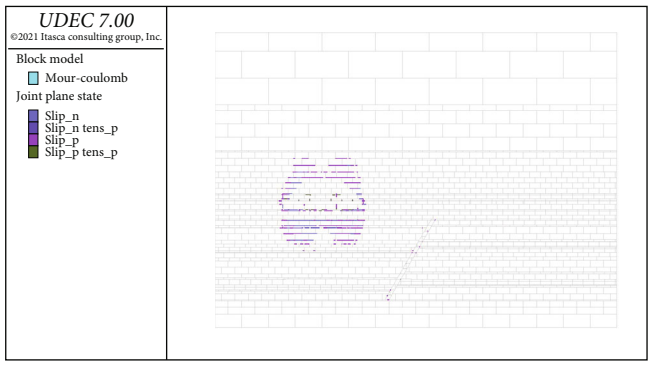

(c) Excavation 60 m

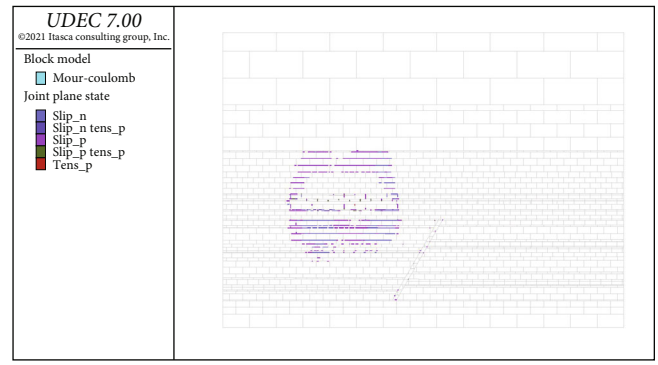

(d) Excavation 80 m

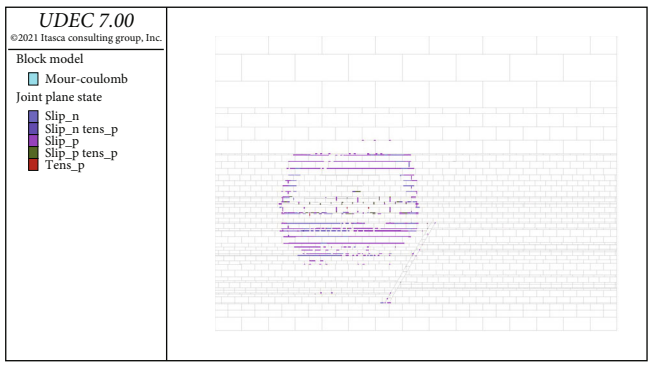

(e) Excavation 100 m

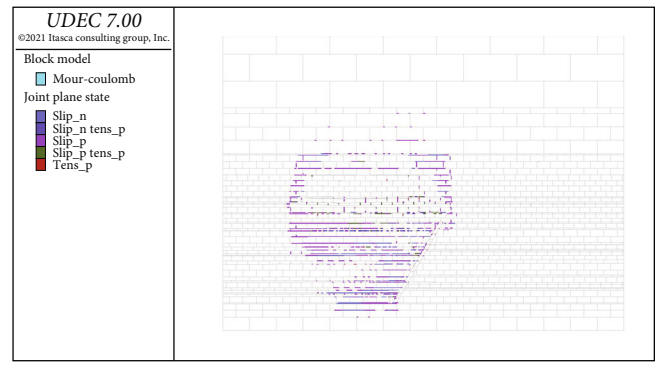

(f) Excavation 120 m

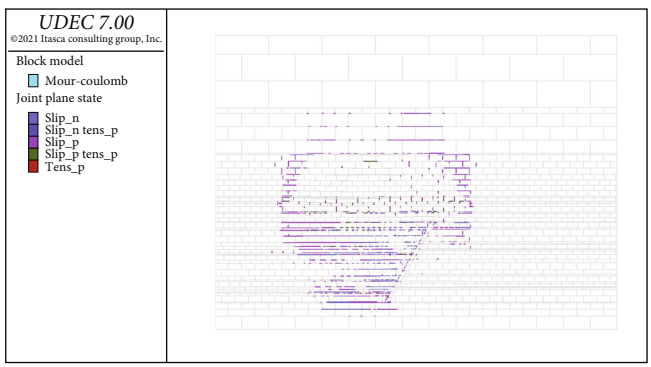

(g) Excavation 140 m

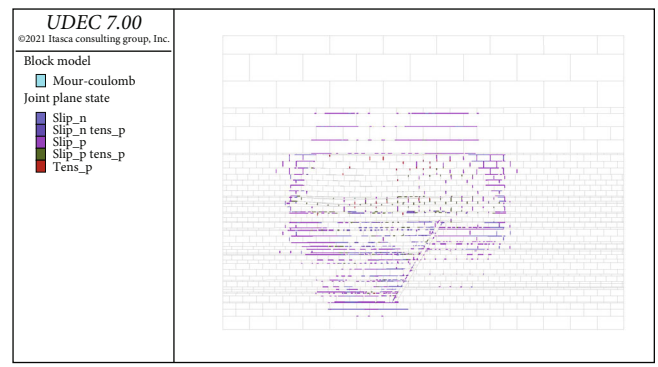

(h) Excavation 160 m

Figure 4: Continued.

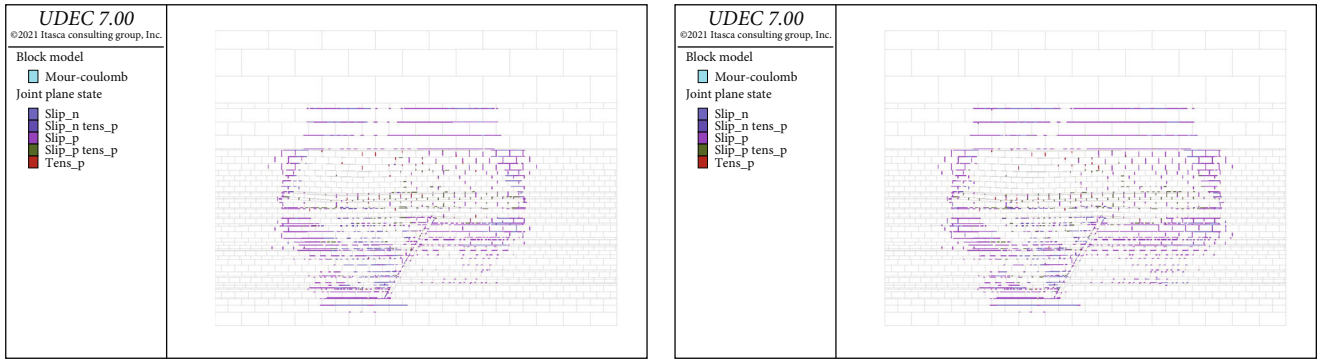

(i) Excavation 180 m (j) Excavation 200 m

Figure 4: Development and distribution map of overlying fissures in No. 5 coal seam.

32]. Box dimension method is the most common method for calculating fractal dimension. The calculation relationship of box dimension can be expressed as [31]

$$\mathrm{Dim}_{\mathrm{box}}(s) = \lim_{r \longrightarrow 0} \frac{\ln N(r)}{\ln r}. \quad (1)$$

Based on this, the box dimension is used to characterize the fractal dimension of the fracture distribution of mining rock. Firstly, the fracture development distribution map is binarized by MATLAB self-compiled language, and then, the fitting relationship between $\ln r$ and $\ln N(r)$ is obtained by MATLAB. The slope of the fitting curve is the fractal box dimension. Figures 6 and 7 show the evolution of mining-induced fractures, the binary map after treatment, and the fractal dimension of No. 5 and No. 9 coal seam excavation 200 m. In order to facilitate the description below, the fractal dimensions of mining-induced fissures in No. 5 and No. 9 coal seams are defined as "fractal dimension 1" and "fractal dimension 2," respectively.

In order to facilitate the analysis and observation, the fractal dimension statistics of No. 5 and No. 9 coal seam excavation at different distances are shown in Tables 1 and 2. It can be seen that the correlation coefficients of all fitting relationships are almost above 0.99, and the fitting degree of the two is relatively high. It shows that the fractal box dimension obtained by this method can better characterize the spatial distribution pattern of mining-induced fractures in the shale, and the larger the fractal dimension is, the more intensive the current fracture development is.

Figure 8 is the relationship between different excavation distances and fractal dimension of No. 5 and No. 9 coal seams. From the change trend of fractal dimension 1 in Figure 6, it can be seen that when No. 5 coal seam is excavated at the beginning, the fractal dimension has a relatively large upward trend in the process of excavation to 20 m to 60 m, indicating that at this time, the new mining-induced rock fractures are the main, and there are few cracks that are penetrated and compacted. Under general mining conditions, the fractal dimension of the later stage should have a slight downward trend under the influence of periodic weighting [30], and the fractal dimension 1 does have a relatively upward trend in this stage. The reason is that the No. 5 coal seam is just excavated to the top of the fault in this stage. Due to the existence of faults, the lithology of the No. 5 coal seam floor in this area is weak. Therefore, the floor cracks began to extend and develop, resulting in a relatively small increase in the fractal dimension at this stage. With the excavation of No. 5 coal seam gradually away from the fault, especially after the excavation to 160 m, the fractal dimension of the mining-induced fissures in the overlying strata presents a gentle fluctuation trend, indicating that the fissures in the overlying strata and floor have developed to the maximum range at this time. Subsequently, with the continuous advance of excavation, the fissures develop along with the excavation, and the development of fissures in height is basically stagnant.

From the variation trend of fractal dimension 2 in Figure 7, it can be seen that the No. 9 coal seam is basically within the pressure relief range of the floor of No. 5 coal seam. Therefore, the variation trend of fractal dimension 2 is relatively stable on the whole, and the fractal dimension has a downward trend after the excavation of No. 9 coal seam to 40 m in local position. The reason is that under the influence of repeated disturbance and fault, the periodic weighting interval becomes smaller, the overlying strata collapses violently, and the large-scale fractures are periodically closed and compacted. Then, with the excavation closer to the fault, the development of mining fractures began to increase, and the fractal dimension also increased. After the excavation of the fault, because the local position of the fault is broken, the mining fracture is closed and compacted quickly with the influence of the periodic weighting and the self-weight of the upper rock layer, and the fractal dimension shows a slight downward trend. After gradually away from the fault, the fractal dimension of the mining fracture shows a normal gentle fluctuation trend. The mining-induced fissures experienced a dynamic evolution process from generation, penetration, closure, expansion, to compaction [31], and the fractal dimension 2 and fractal dimension 1 of the mining-induced fissures under the influence of repeated disturbance have roughly the same increasing trend.

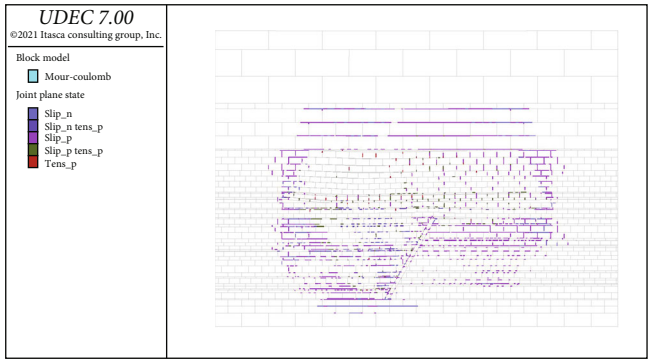

(a) Excavation 20 m

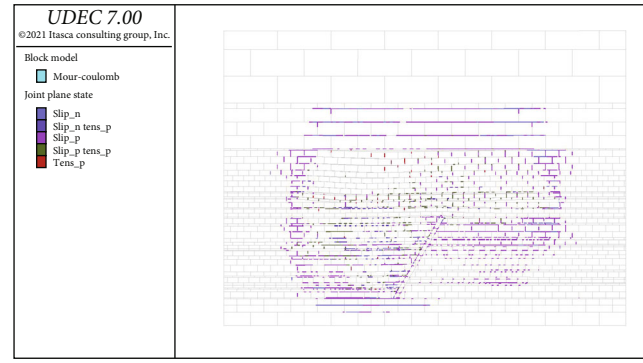

(b) Excavation 40 m

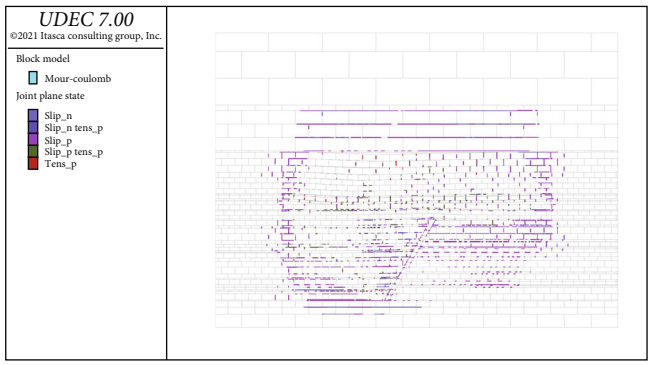

(c) Excavation 60 m

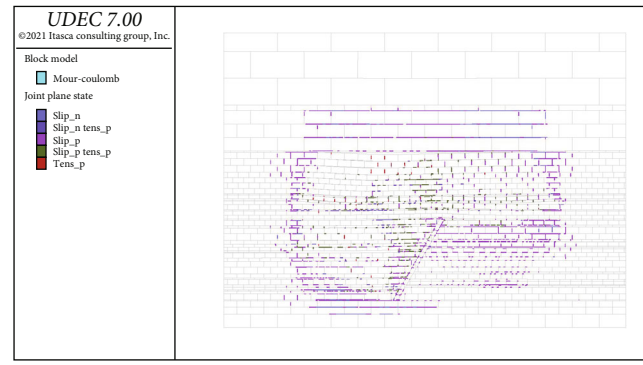

(d) Excavation 80 m

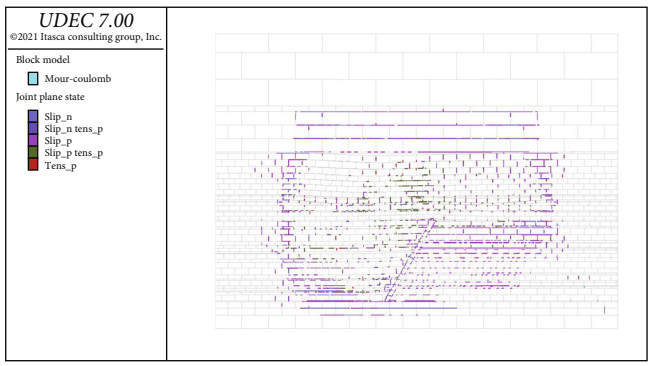

(e) Excavation 100 m

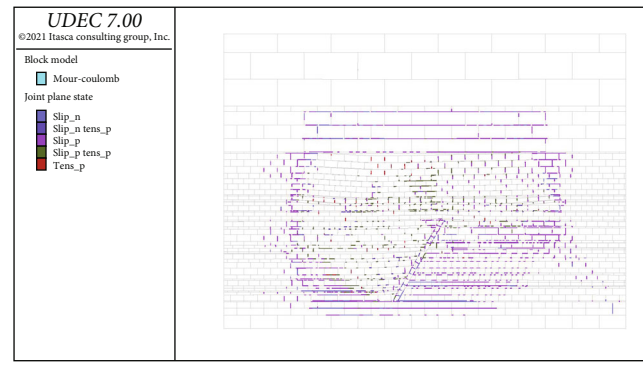

(f) Excavation 120 m

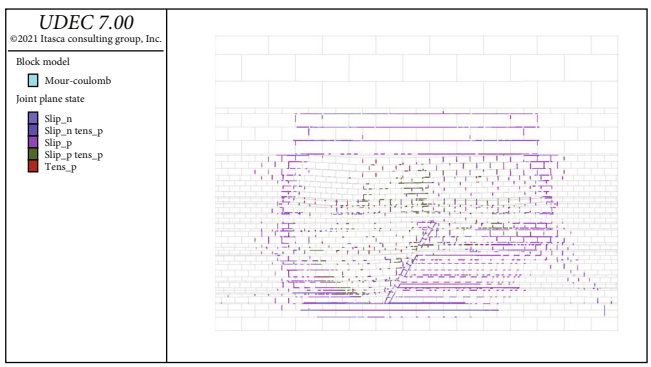

(g) Excavation 140 m

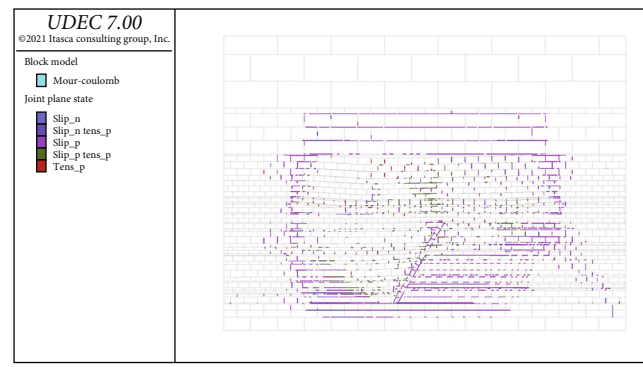

(h) Excavation 160 m

Figure 5: Continued.

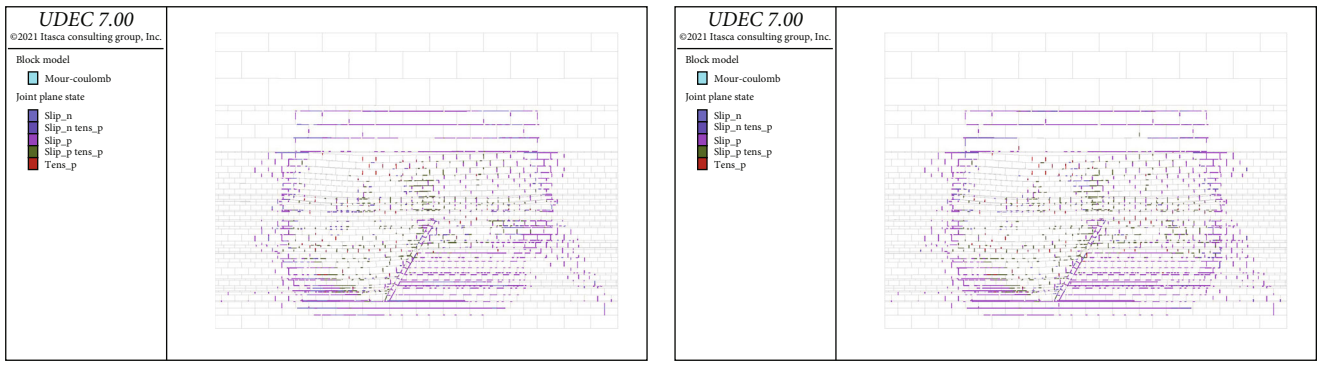

(i) Excavation 180 m (j) Excavation 200 m

Figure 5: Development map of overburden fissures in working face directly through fault excavation.

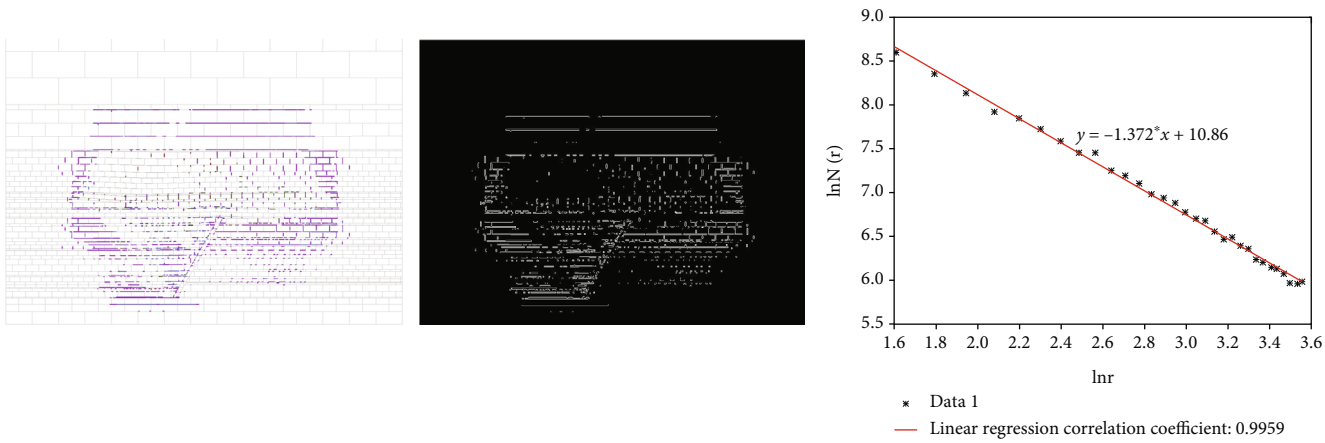

Figure 6: Evolution, binary map, and fractal dimension of overburden fissures in No. 5 coal seam excavation of 200 m.

3. Simulation of Gas Migration in Mining Fracture Field under Normal Fault Conditions

3.1. Mathematical Model of Gas Migration in Mining Fracture Field

3.1.1. Continuous Mathematical Equation of Mining Pressure Relief Gas Flow. Under the influence of mining effect, a large amount of adsorbed gas is transformed into free gas, which is also the key to gas extraction. The flow process of gas after pressure relief can be summarized as gas desorption stage, gas diffusion stage, and gas seepage stage. In the three stages of the whole process of pressure relief gas flow, it covers the diffusion and seepage of free gas and adsorbed gas. Therefore, combined with the law of conservation of mass, the coupling continuous equations of gas diffusion and seepage are expressed as follows:

$$\frac{\partial(\rho_k\varphi_k)}{\partial t}+\nabla\cdot(\rho_k V_k)+\nabla\cdot(\rho_s V_s)+\frac{\partial(\rho_s\varphi_s)}{\partial t}=0, \quad (2)$$

where bottom k, s corresponds to diffusion and seepage, respectively.

Considering that the change rate of gas fluid density with space is much smaller than that with time, which can be ignored, Equation (1) can be simplified as

$$\varphi_k\frac{\partial\rho_k}{\partial t}+\rho_k\,\mathrm{div}\,V_k+\varphi_s\frac{\partial\rho_s}{\partial t}+\rho_s\,\mathrm{div}\,V_s=0. \quad (3)$$

3.1.2. Mining Pressure Relief Gas Flow Equation. The Reynolds number of pressure relief gas flow in the areas with small fractures and pores of coal and rock mass is between 1 and 10, belonging to laminar flow; when Reynolds number of pressure relief gas flow increases to 10~100, gas flow state is between laminar and turbulent nonlinear seepage (also called transition flow). When Reynolds number of pressure relief gas flow is greater than 100, gas flow transits from laminar flow to turbulent flow. Therefore, Darcy's law, Navier-Stokes equation, and Brinkman's equation are used to describe the flow equations of gas fluid in front of working face (uncut coal body), working face, roadway, and goaf area, respectively [32].

(1) Gas Flow Equation in front of Coal Mining. The permeability of most coal seams in Guizhou coal mines is low. The flow of gas in low permeability coal seams needs

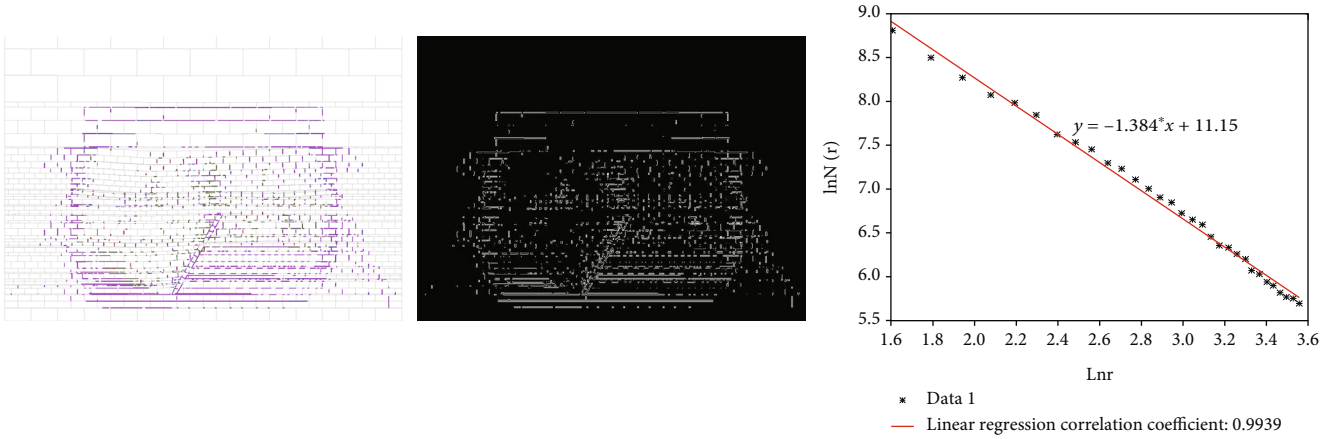

Figure 7: Evolution, binary map, and fractal dimension of 200 m overburden fissures in No. 9 coal seam excavation.

Table 1: Fractal dimension statistics at different excavation distances for coal seam No. 5.

Excavation distance (m)	Fitting relationship	Correlation coefficient (R^2)	Excavation distance (m)	Fitting relationship	Correlation coefficient (R^2)
20	$\ln N(r) = 6.687 - 1.053 \ln r$	0.9584	120	$\ln N(r) = 10.26 - 1.384 \ln r$	0.9973
40	$\ln N(r) = 8.141 - 1.222 \ln r$	0.9920	140	$\ln N(r) = 10.38 - 1.371 \ln r$	09971
60	$\ln N(r) = 9.011 - 1.314 \ln r$	0.9921	160	$\ln N(r) = 10.52 - 1.347 \ln r$	0.9964
80	$\ln N(r) = 9.565 - 1.364 \ln r$	0.9932	180	$\ln N(r) = 10.71 - 1.363 \ln r$	0.9948
100	$\ln N(r) = 9.782 - 1.369 \ln r$	0.9921	200	$\ln N(r) = 10.86 - 1.372 \ln r$	0.9959

Table 2: Fractal dimension statistics at different excavation distances for coal seam No. 9.

Excavation distance (m)	Fitting relationship	Correlation coefficient (R^2)	Excavation distance (m)	Fitting relationship	Correlation coefficient (R^2)
20	$\ln N(r) = 10.93 - 1.377 \ln r$	0.9947	120	$\ln N(r) = 11.06 - 1.369 \ln r$	0.9945
40	$\ln N(r) = 11.01 - 1.392 \ln r$	0.9958	140	$\ln N(r) = 11.08 - 1.368 \ln r$	09946
60	$\ln N(r) = 10.90 - 1.356 \ln r$	0.9944	160	$\ln N(r) = 11.06 - 1.362 \ln r$	0.9945
80	$\ln N(r) = 10.95 - 1.361 \ln r$	0.9943	180	$\ln N(r) = 11.09 - 1.372 \ln r$	0.9945
100	$\ln N(r) = 11.05 - 1.375 \ln r$	0.9945	200	$\ln N(r) = 11.15 - 1.384 \ln r$	0.9939

to consider the Klinkenberg effect [33]. The gas gravity is small and can be ignored in the calculation. According to the Darcy law, coal gas seepage velocity can be expressed as

$$v = -\frac{k}{\mu}\left(1 + \frac{h}{p}\right) \cdot \nabla p, \tag{4}$$

where v is gas seepage velocity, m/s; μ is gas dynamic viscosity; and h is the Klinkenberg coefficient, Pa.

The permeability of coal in front of coal mining is mainly related to the effective stress. Considering the change of gas pressure and the adsorption effect of adsorbed gas, the dynamic equation of permeability is

$$k = \frac{k_0}{1 + \varepsilon_v}\left[1 + \frac{\varepsilon_v}{\varphi_0} + \frac{K_y \Delta p(1 - \varphi_0)}{\varphi_0} - \frac{2a\rho_v RTK_y}{9V_m\varphi_0} \ln \frac{(1 + bp)}{(1 + bp_0)}\right]^3, \tag{5}$$

where k_0 is the initial permeability of coal, m^2; ε_v is the volumetric strain of coal; φ_0 is the initial porosity of coal, %; K_y is the coal skeleton compression coefficient, 1/MPa; p_0 is the initial gas pressure of coal body, Pa; a is the limit gas adsorption capacity of unit mass coal, m^3/t; ρ_v is the coal density, kg/m^3; R is the ideal gas constant; T is the absolute temperature in standard conditions, $T = 273$ K; V_m is the total volume of coal, kg/m^3; p is the gas pressure, Pa; and b is the absorption of coal, 1/MPa.

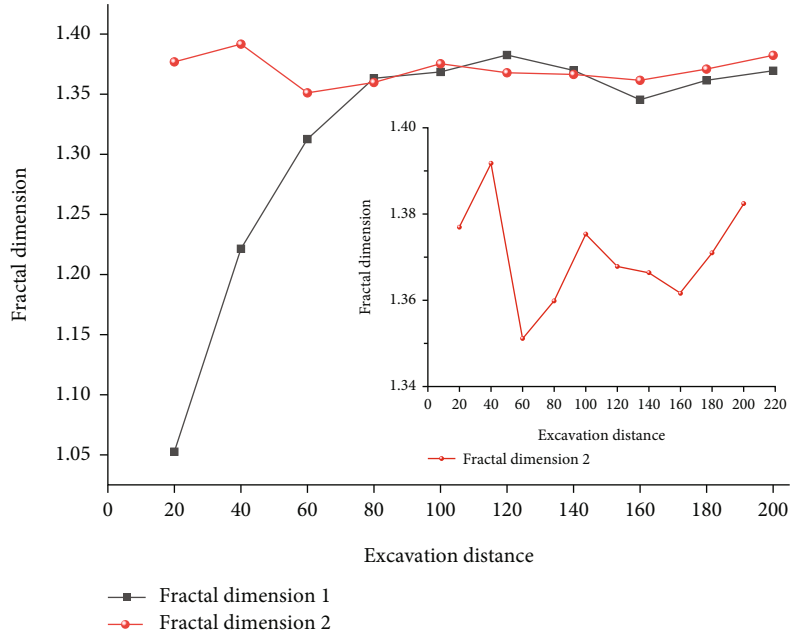

Figure 8: Relationship between different excavation distances and fractal dimension variation in coal seam No. 5 and No. 9.

(2) Gas Flow Equation of Coal Mining Face and Roadway. The velocity of gas in coal mining face and roadway is fast, which can be described by the Navier-Stokes equation. The Navier-Stokes equation can be expressed as

$$-\nabla \cdot \eta\left[\nabla u_{\mathrm{ns}} + (\nabla u_{\mathrm{ns}})^{T}\right] - \rho(u_{\mathrm{ns}} \cdot \nabla)u_{\mathrm{ns}} + \nabla P_{\mathrm{ns}} = 0, \quad \nabla \cdot u_{\mathrm{ns}} = 0, \tag{6}$$

where u is the rate of curve of flow of fluid, m/s, and η is the coefficient of viscosity, kg/(m·s).

(3) Gas Flow Equation of Mining-Induced Fracture Field. The gas flow law of mining-induced fracture field can be described by the Brinkman motion equation, which is expressed as

$$-\nabla \cdot \eta\left[\nabla u_{\mathrm{br}} + (\nabla u_{\mathrm{br}})^{T}\right] - \left(\frac{\eta}{k}u_{\mathrm{br}} + \nabla P_{\mathrm{br}} - F\right) = 0, \quad \nabla \cdot u_{\mathrm{br}} = 0. \tag{7}$$

(4) Diffusion-Convection Equation of Gas in Coal.

$$\theta_s \frac{\partial I}{\partial t} + \nabla \cdot (-\theta_s D_L \nabla I + uI) = S_I, \tag{8}$$

where θ_s is the volume rate of gas fluid; I is the concentration of gas dissolution, kg/m^3; D_L is the tensor of pressure diffusion, m^2/d; and S_I is the relative gas emission rate, m^3/t.

The gas diffusion flow can be described by Fick's law. The gas diffusion flow equation in coal pores can be expressed as

$$J = -D\frac{\partial W}{\partial n}, \tag{9}$$

where J is the diffusion velocity of gas, m^3/m^{2}s; D is the diffusion coefficient of gas, m^2/s; W is the concentration of gas, m^3/t; and n is the diffusion distance of gas, m.

3.2. Construction of Numerical Simulation Model. The existence of faults destroys the "trapezoidal" caving form of intrusive rocks on both sides of the fault, and the development is not continuous. However, since the No. 9 coal seam is at the high position of the fault, with the continuous development of the mining fracture height, the mining fracture of the upper working face will develop along the direction of the top of the fault to the bottom. A simple three-dimensional trapezoidal table can be approximately constructed to characterize the goaf of the fault tectonic area, as shown in Figure 9, so as to model and simulate the numerical simulation.

The gas migration in the mining fracture field mainly considers the fracture zone and caving zone in the vertical three zones of the mining fracture. According to the actual working conditions of the coal mining face in mine in Guizhou, a simple rectangular trapezoidal table physical model of the mining rock fracture in No. 5 coal seam and No. 9 coal seam is drawn by UG mapping software, as shown in Figure 10. The physical model is divided into different regions according to the broken expansion coefficient of the rock collapse.

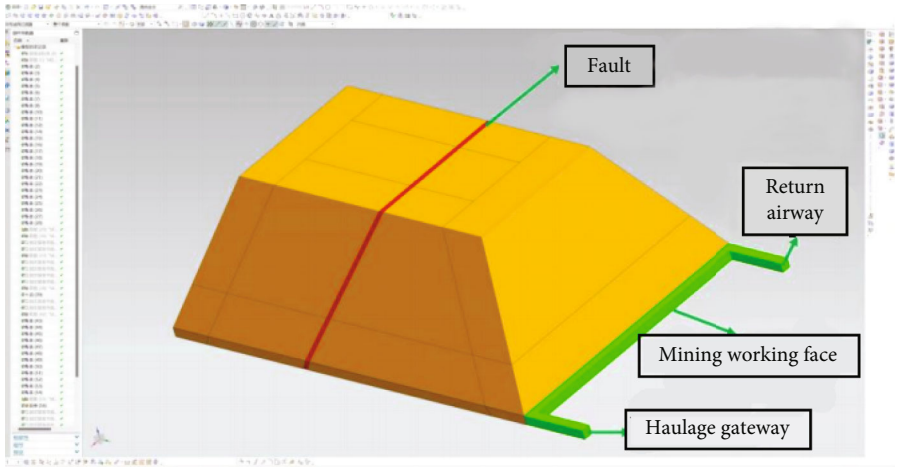

Figure 9: Sketch map of the mining area in the fault structure area.

3.3. Simulation Hypothesis of Porous Media for Mining-Induced Fractures. A large number of fractures will be generated in overlying strata after coal seam mining, which is called secondary mining fractures [34]. Secondary mining fractures and coal-rock joints, bedding, and primary fractures formed in the process of coal-forming constitute the fracture system of mining rock.

The random distribution of secondary mining fractures is mainly related to the key strata, adjacent rock lithology, mining height, and secondary repeated mining stress. The primary fracture is formed by coal and rock under the original geological action. The average channel size, permeability, and porosity of the fracture are several orders of magnitude smaller than those of the mining-induced fracture. Therefore, the secondary mining-induced fracture is the main channel for gas migration in the mining-induced rock fracture system.

After mining, the mechanical properties of coal and rock mass caused by erosion rock breaking and stress redistribution have changed greatly. However, due to the randomness of fracture structure and collapse accumulation mode of weathered rock after mining, the migration of gas and other mixed gases in weathered rock fractures is not affected in essence. Therefore, it is considered that the fracture zone and caving zone after mining-induced erosion rock breaking have the properties of porous media. According to the definition of porous media and seepage mechanics, the characteristics of porous media of mining-induced fissures are described as follows. (1) Macroscopically, erosion rock fissures can still be regarded as continuous isotropic media, and fissures are equivalently replaced by porous media. (2) The weathered rock fissures can be studied as a whole, which is composed of coal, rock, gas, and other mixed gases and fissures. (3) The gap between the strata in the rock fracture is interconnected, and the range of the whole rock fracture field is relatively narrow.

3.4. Numerical Model Setting and Meshing. In COMSOL numerical simulation, two physical field interfaces of "free and porous media flow" and "porous media rare material transfer" were selected to set the physical model, and the solver was set to meet the requirements of iterative solution. The solution step was transient. In order to ensure the rationality of the numerical simulation results, the grid division was encrypted at the local position of the fault, and its location was relatively sparse. The grid division of the two physical models is shown in Figure 11.

The location of the transport lane is set as the inlet boundary, and the flow rate of fresh air is set as 2.3 m/s. The return airway position is set to the outlet boundary of pressure difference flow, and the solid boundary is set to the "wall" in the physical field of free and porous media flow. The regions divided by the physical model are set by using permeability and porosity to characterize the rock dilatancy coefficient. The mining fracture field has the properties of porous media. The relationship between permeability, porosity, and rock dilatancy coefficient can be expressed by the Blake-Kozeny formula as follows:

$$k = \frac{\varphi_n^{\,3} d_m^{\,2}}{150(1-n)^2}, \tag{10}$$

where φ_n is the porosity, $\varphi_n = 1 - (1/K_p)$; K_p is the rock breaking coefficient of mining fracture field; and d_m is the average diameter of porous media particles, m.

In the numerical simulation, in order to simplify the analysis, the gas emission in the mining-induced fracture field is regarded as uniform distribution, so the calculation method of gas source term in each region in the physical model is as follows:

$$Q_s = \frac{Q_g \rho}{60 V_a}, \tag{11}$$

where Q_s is the gas source term of each region, kg/m^{3}s; Q_g is the gas emission of gas source term in each region, m^3/min; and V_a is the volume of the source term in each region, m^3.

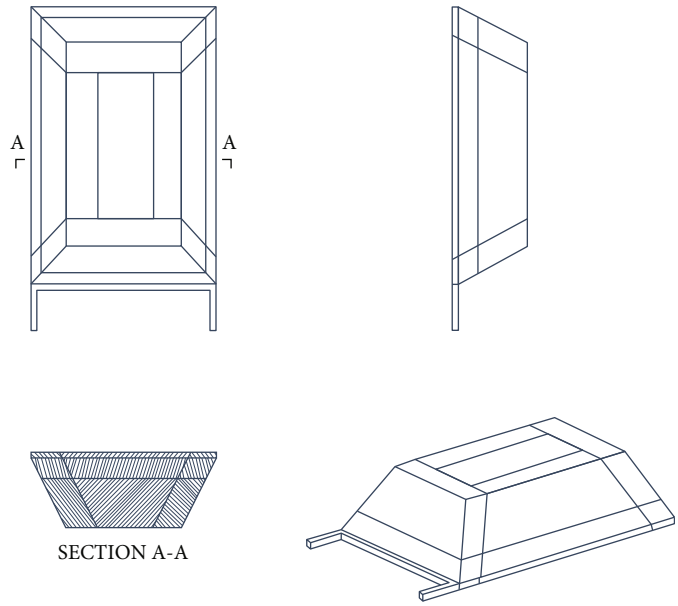

(a) No. 5 coal seam

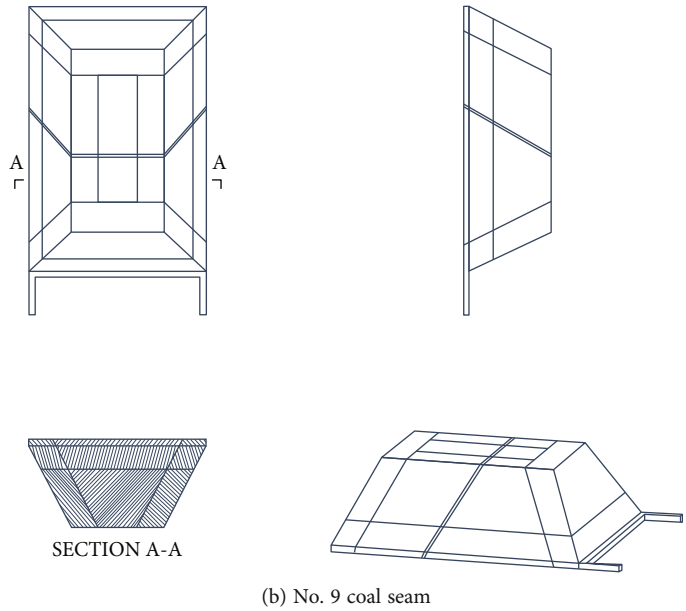

(b) No. 9 coal seam

Figure 10: Rectangular trapezoidal platform of overburden fissures of mined coal seam.

3.5. Gas Migration Numerical Simulation Results and Analysis. Without the influence of faults, the gas spatial migration distribution results of simulated mining-induced fracture field in No. 5 coal seam are shown in Figure 12. It can be seen that the gas accumulation in the upper corner is more serious. The reason is that there is a concentration difference and density difference between the gas and the surrounding air, so there is an area where the gas cannot be completely taken away by the fresh air flow in the coal mine excavation and mining space, and the pressure relief gas has good floating characteristics. Due to the effect of floating, a certain amount of gas accumulates at a certain height of fracture development, especially under the condition of U-type ventilation, the gas accumulates in the upper corner. At the same time, it can be seen that due to the influence of air leakage on the mining face, the gas concentration on the side of the return airway will gradually increase, and the pressure relief gas in the goaf will rise and float in the mining fracture field and migrate to the separated layer development area of the overlying strata. Combined with Figure 13, it can not only clearly see the gas migration law but also can be seen that the gradient of gas concentration near the coal mining face changes greatly, and the gradient gradually decreases when it is far away from the coal mining face. In the whole mining fracture field, the gas concentration in the most inner return airway side of the goaf is the largest.

It can be seen from Figure 14 that the spatial distribution of gas migration in the mining fracture field in the fault structure area is generally consistent with the spatial

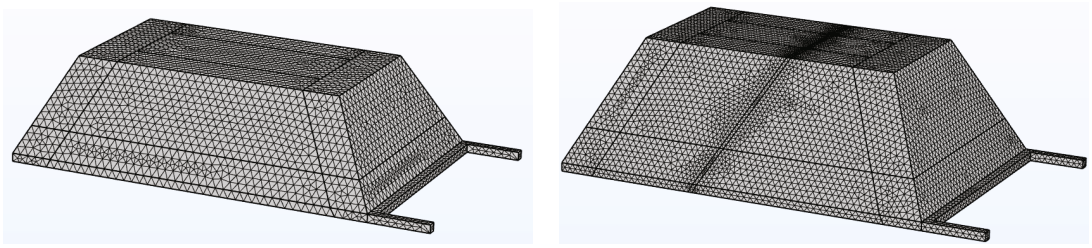

(a) No. 5 coal seam (b) No. 9 coal seam

Figure 11: COMSOL numerical model meshing.

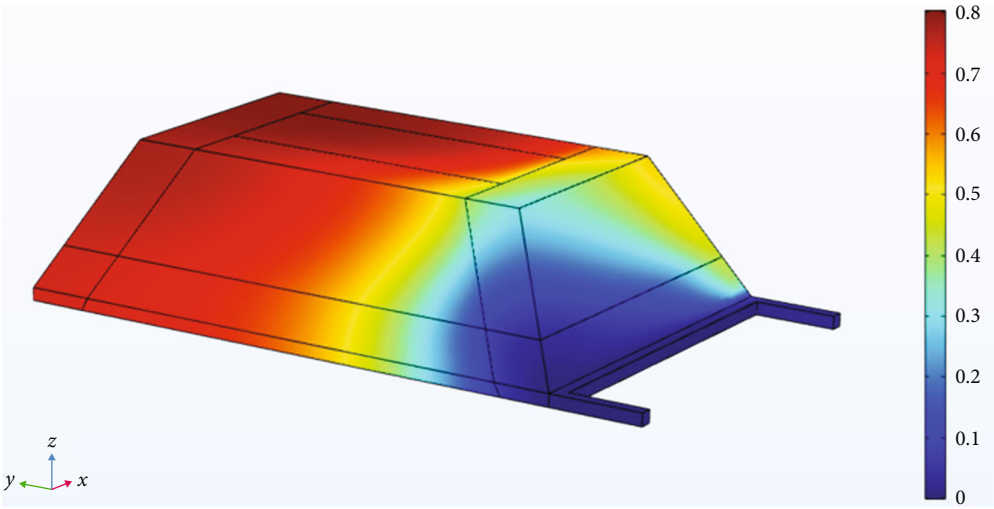

Figure 12: Spatial gas transport distribution in the mining fissure field of No. 5 coal seam.

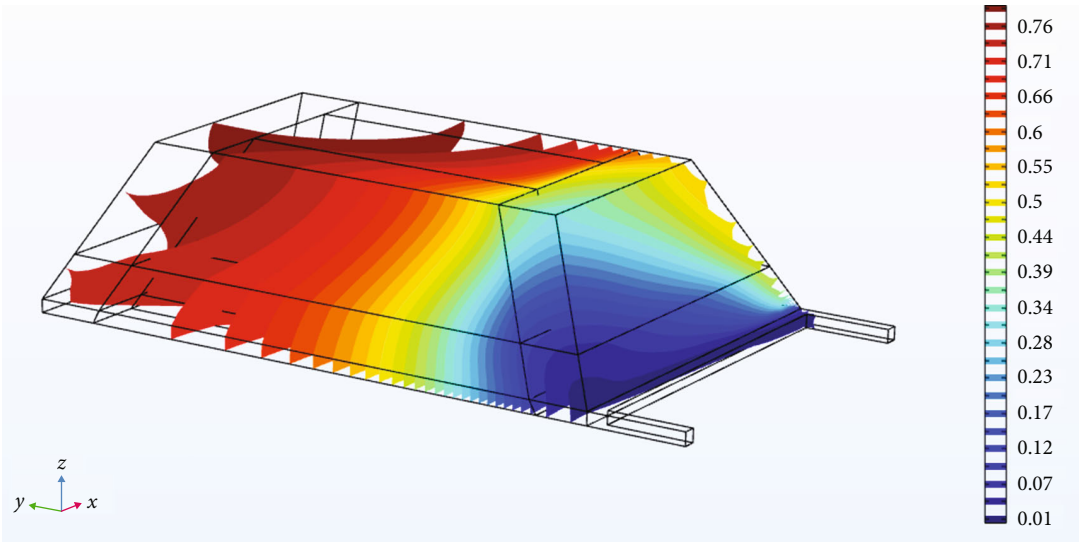

Figure 13: Contour map of gas spatial transport distribution in the mining fissure field of No. 5 coal seam.

distribution of gas migration in the mining fracture field without fault structure shown in Figure 12. The maximum concentration of gas still appears on the other side of the goaf. However, it can be seen that although No. 9 coal seam is in the range of pressure relief of No. 5 coal seam mining, due to the existence of faults, it still leads to high gas concentration in the mining fracture field of No. 9 coal seam goaf. Figure 15 shows the spatial distribution of gas migration in the mining-induced fracture field in the fault structure area. Comparing Figure 13, it can be

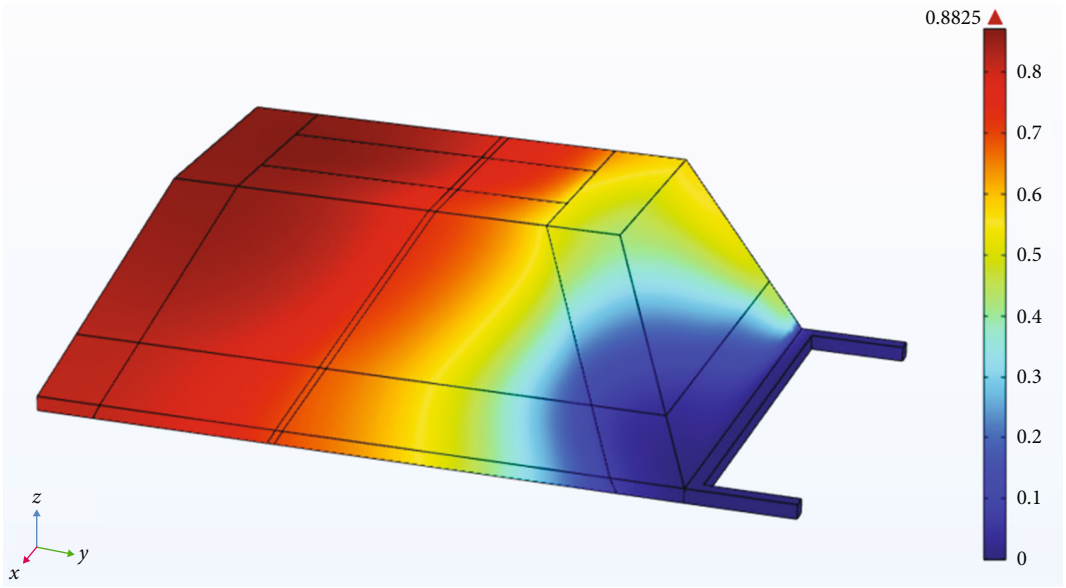

Figure 14: Spatial gas transport distribution in mining fissure fields in fault-tectonic regions.

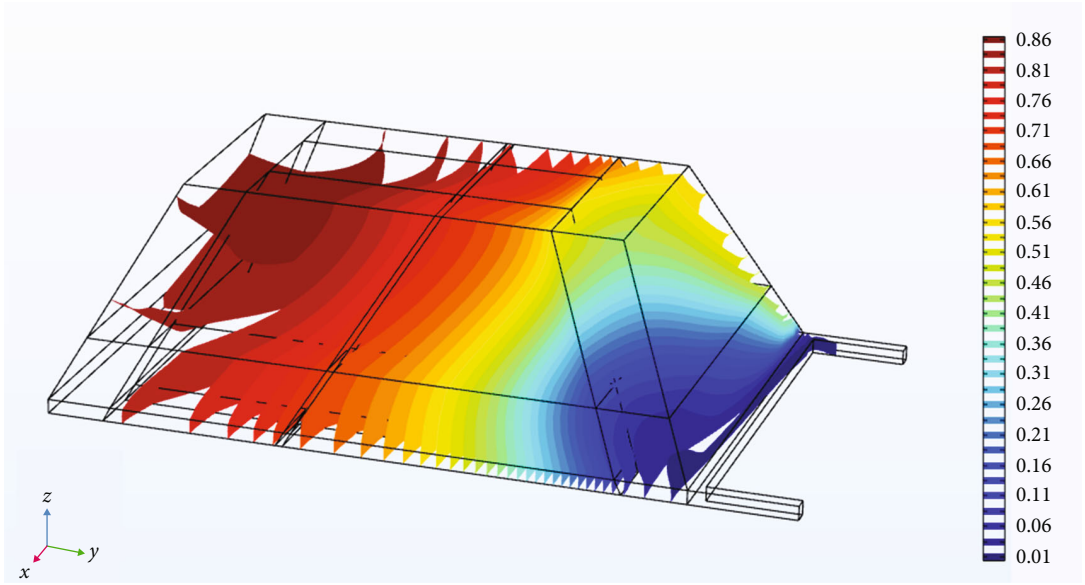

Figure 15: Contour map of gas spatial transport distribution in mining fracture field in the fault-tectonic region.

seen that the variation gradient of gas concentration in the whole mining-induced fracture field of No. 9 coal seam is larger than that of No. 5 coal seam. At the same time, the gas concentration in different fault layers is also different in the whole fault area. The gas concentration in the high level of the fault is slightly larger than that in the low level of the fault. Compared with the fracture (Figure 5), it can be seen that the compaction area near the high level of the fault is larger, the compaction area in the low level of the fault is relatively small, and the fracture is more developed than the high level area. Figure 16 clearly shows the spatial migration and distribution characteristics of gas in the mining-induced fracture field in the fault structure area under different slice angles. It can be seen that the gas concentration is relatively high near the fault structure area, indicating that even if the fault is located in the mining pressure relief range of No. 5 coal seam, the gas will still accumulate near the fault structure.

In order to further analyze the influence of fault structure on gas migration in mining fracture field, the flow line of gas flow direction in mining fracture field in fault structure area is derived as shown in Figure 17. It can be seen that the gas flow curve is complex on the whole, which is in line with the basic law of the complexity of gas migration in the mining fracture field. At the same time, it can be seen that a large number of gas flow near the fault location and gather more actively, indicating that the existence of faults has a greater impact on gas migration. It can be seen from the

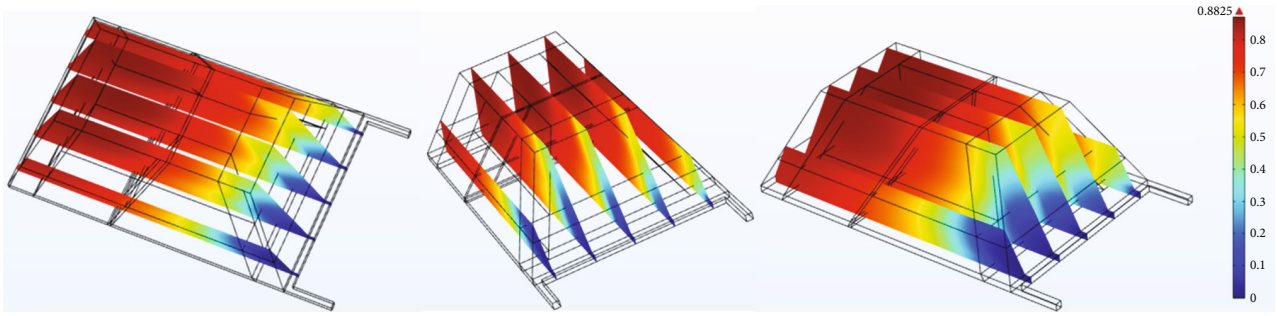

Figure 16: Different angle slices of gas spatial transport distribution in the mining fissure field in the fault-tectonic region.

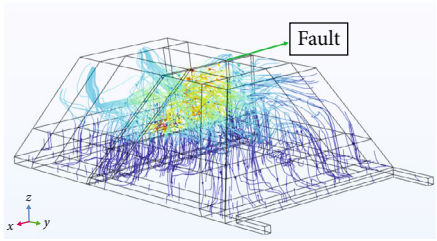

Figure 17: Directional map of gas flow in the fault structure area.

gas flow line of the coal mining face that the gas in the goaf near the coal mining face diffuses towards the coal mining face with the air leakage flow of the coal mining face, which is consistent with the gas emission law of the field working face.

4. Conclusions

(1) Through the simulation of the fracture development of close coal seam under the influence of faults, it can be seen that the fault is less affected by the mining of No. 5 coal seam. The fractures near the upper plate of the underlying fault of No. 5 coal seam are relatively developed, and the fracture development in the lower plate of the fault is not obvious. Under the influence of faults, the mining of No. 9 coal seam causes a large number of new mining-induced fractures in the fault area. With the mining of No. 9 coal seam moving forward, the mining-induced fractures develop along the direction of the top of the fault to the bottom, and the mining-induced fractures experience the development process of "development-expansion-compaction"

(2) Through the binarization processing and quantitative analysis of the distribution of mining-induced fissures in No. 5 and No. 9 coal seams, it can be seen from the overall trend of fractal dimension that the mining-induced fissures have experienced a dynamic evolution process from generation, penetration, closure, expansion, to compaction, and the fractal dimension of mining-induced fissures in No. 5 and No. 9 coal seams has roughly the same increasing trend under the influence of repeated disturbances

(3) By constructing the three-dimensional trapezoidal platform model of No. 5 and No. 9 coal seam mining fractured rock, the numerical simulation analysis of gas migration in mining fractured field under the influence of fault is carried out. Under the condition of U-type ventilation, the gas accumulation in the upper corner of the mining fracture field is serious, and the gas concentration in the fracture development zone of the overlying strata is higher. On the whole, the gradient of gas concentration near the working face in the mining-induced fracture field changes greatly. When it is far away from the working face, the gradient gradually becomes smaller. In the whole mining-induced fracture field, the gas concentration at the return airway side in the innermost goaf is the largest

(4) Through the simulation and comparative analysis of No. 5 coal seam and No. 9 coal seam, the results show that the spatial distribution of gas migration in the mining fracture field in the fault structure area is generally consistent with that in the mining fracture field without fault structure, and the maximum concentration of gas still appears on the other side of the goaf. Due to the existence of faults, the gas concentration of mining-induced fracture field in goaf of No. 9 coal seam is high. Even in the pressure relief range of No. 5 coal seam, the gas concentration of mining-induced fracture field in goaf is still high and the variation gradient is large. The gas will still accumulate and circulate actively near the fault structure. The gas concentration at the high level of the fault is slightly higher than that at the low level

Data Availability

The data used to support the findings of this study are available from the corresponding author upon request.

Conflicts of Interest

The authors declare that they have no conflicts of interest.

Acknowledgments

The study was supported by the National Natural Science Foundation (52064009) and the Open Fund Project of Key Laboratory of Safe and Effective Coal Mining, Ministry of Education (JYBSYS2021206).

References

[1] H. P. Xie, L. X. Wu, and D. Z. Zheng, "Prediction on the energy consumption and coal demand of China in 2025," *Journal of China Coal Society*, vol. 44, no. 7, pp. 1949–1960, 2019.

[2] H. Zhang, Y. P. Cheng, L. Yuan, and Z. J. Pan, "Hydraulic flushing in soft coal sublayer: gas extraction enhancement mechanism and field application," *Energy Science & Engineering*, vol. 7, no. 5, pp. 1970–1993, 2019.

[3] E. Y. Wang, C. Peng, Z. T. Liu, Y. Y. Liu, Z. H. Li, and X. L. Li, "Fine detection technology of gas outburst area based on direct current method in Zhuxianzhuang Coal Mine, China," *Safete Science*, vol. 115, pp. 12–18, 2019.

[4] C. Mark, "Coal bursts that occur during development: a rock mechanics enigma," *International Journal of Mining Science and Technology*, vol. 28, no. 1, pp. 35–42, 2018.

[5] W. Li, T. W. Ren, A. Busch et al., "Architecture, stress state and permeability of a fault zone in Jiulishan coal mine, China: Implication for coal and gas outbursts," *International Journal of Coal Geology*, vol. 198, pp. 1–13, 2018.

[6] J. Y. Lin, Y. J. Zhou, K. Zhang et al., "Coal and gas outburst affected by law of small fault instability during working face advance," *Geofliuds*, vol. 2020, Article ID 8880091, 12 pages, 2020.

[7] W. Gong and D. Guo, "Control of the tectonic stress field on coal and gas outburst," *Applied Ecology and Environmental Research*, vol. 16, no. 6, pp. 7413–7433, 2018.

[8] C. J. Fan, S. Li, M. K. Luo, W. Z. Du, and Z. H. Yang, "Coal and gas outburst dynamic system," *International Journal of Mining Science and Technology*, vol. 27, no. 1, pp. 49–55, 2017.

[9] R. Zhang, Y. P. Cheng, L. Yuan, H. X. Zhou, W. Liang, and W. Zhao, "Enhancement of gas drainage efficiency in a special thick coal seam through hydraulic flushing," *International Journal of Rock Mechanics and Mining Sciences*, vol. 124, article 104085, 2019.

[10] L. Yuan, "Control of coal and gas outbursts in Huainan mines in China: a review," *Journal of Rock Mechanics and Geotechnical Engineering*, vol. 8, no. 4, pp. 559–567, 2016.

[11] C. Zhai, X. W. Xiang, J. Xu, and S. L. Wu, "The characteristics and main influencing factors affecting coal and gas outbursts in Chinese Pingdingshan mining region," *Natural Hazards*, vol. 82, no. 1, pp. 507–530, 2016.

[12] Y. Xue, J. Liu, X. Liang, S. Wang, and Z. Ma, "Ecological risk assessment of soil and water loss by thermal enhanced methane recovery: numerical study using two-phase flow simulation," *Journal of Cleaner Production*, vol. 334, article 130183, 2022.

[13] C. J. Zhu and B. Q. Lin, "Effect of igneous intrusions and normal faults on coalbed methane storage and migration in coal seams near the outcrop," *Natural Hazards*, vol. 77, no. 1, pp. 17–38, 2015.

[14] "Normal faults and gas migration in an active plate boundary, southern Taranaki Basin, offshore New Zealand," *AAPG Bulletin*, vol. 96, no. 9, pp. 1733–1756, 2012.

[15] Z. X. Li, "Study on numerical simulation of gas emission regularity and boundary condition of the goaf in coal caving of the fully-mechanized," *Journal of China Coal Society*, vol. 2, pp. 173–178, 2002.

[16] Z. X. Li, S. L. Ji, and Z. Y. Ti, "Two-phase miscible diffusion model and its solution between gas in goaf and atmosphere," *Chinese Journal of Rock Mechanics and Engineering*, vol. 16, pp. 2971–2976, 2005.

[17] Q. Lu and G. Huang, "A simulation of gas migration and control in goaf based on multi-components LBM," in *2009 4th International Conference on Computer Science & Education*, pp. 435–440, Nanning, China, 2009.

[18] WQ, "Study on seepage theory in overbroken rock mass and its application," *Chinese Journal of Rock Mechanics and Engineering*, vol. 8, p. 1262, 2003.

[19] C. Zhao and S. Valliappan, "Finite element modelling of methane gas migration in coal seams," *Journal of Natural Gas Science and Engineering*, vol. 55, no. 4, pp. 625–629, 1995.

[20] S. G. Li, P. Xiao, H. Y. Pan, H. F. Cheng, and L. Hua, "Experimental investigation on the seepage law of pressure-relieved gas under the influence of mining," *Safety Science*, vol. 50, no. 4, pp. 614–617, 2012.

[21] S. G. Li, H. F. Lin, P. X. Zhao, P. Xiao, and H. Y. Pan, "Dynamic evolution of mining fissure elliptic paraboloid zone and extraction coal and gas," *Journal of China Coal Society*, vol. 39, no. 8, pp. 1455–1462, 2014.

[22] Z. H. Zhu, T. Feng, Z. G. Yuan, D. H. Xie, and W. Chen, "Solid-gas coupling model for coal-rock mass deformation and pressure relief gas flow in protection layer mining," *Advances in Civil Engineering*, vol. 2018, Article ID 5162628, 6 pages, 2018.

[23] S. G. Gao, F. Luo, Y. B. Liu, P. Gou, and G. D. Li, "Gas migration of coal in front of a mining face considering crack evolution," *Environmental Earth Sciences*, vol. 75, no. 18, 2016.

[24] H. Yang, Z. Liu, D. Zhu, W. Yang, D. Zhao, and W. Wang, "Study on the fractal characteristics of coal body fissure development and the law of coalbed methane migration of around the stope," *Geofluids*, vol. 2020, Article ID 9856904, 15 pages, 2020.

[25] C. Cheng, X. Y. Cheng, R. Yu, W. P. Yue, and C. Liu, "The law of fracture evolution of overlying strata and gas emission in goaf under the influence of mining," *Geofluids*, vol. 2021, Article ID 2752582, 16 pages, 2021.

[26] L. Yuan, "Theory of pressure-relieved gas extraction and technique system of integrated coal production and gas extraction," *Journal of China Coal Society*, vol. 34, no. 1, pp. 1–8, 2009.

[27] J. Cao and W. P. Li, "Numerical simulation of gas migration into mining-induced fracture network in the goaf," *International Journal of Mining Science and Technology*, vol. 27, no. 4, pp. 681–685, 2017.

[28] L. Wang, C. L. Hu, J. W. Zhang, and G. Y. Chen, "Correlation between the structural characteristics of the deep four-liver fault and the important mineral deposits in Guizhou province," *Journal of Geomechanics*, vol. 25, no. 1, pp. 36–51, 2019.

[29] G. M. Yu, H. P. Xie, H. W. Zhou, Y. Z. Zhang, and L. Yang, "Experimental study on the distribution law and fractal property of mining fractures in structured rock mass," *Journal of Experimental Mechanics*, vol. 2, pp. 14–23, 1998.

[30] Y. X. Zhao, C. W. Ling, B. Liu, and X. He, "Fracture evolution and energy dissipation of overlying strata in shallow-buried

underground mining with ultra-high working face," *Journal of Mining & Safety*, vol. 38, no. 1, pp. 9–18+30, 2021.

[31] B. B. Yang, S. C. Yuan, D. Z. Zheng et al., "Spatial and temporal characteristics of overburden fractures due to repeated mining in close distance coal seams," *Journal of Mining & Safety Engineering*, vol. 39, no. 2, pp. 255–263, 2020.

[32] T. H. Yang, S. K. Chen, W. C. Zhu, M. Z. Meng, and Y. F. Gao, "Water inrush mechanism in mines and nonlinear flow model for fractured rocks," *Chinese Journal of Rock Mechanics and Engineering*, vol. 7, pp. 1411–1416, 2008.

[33] S. G. Cao, P. Guo, Y. Li, Y. J. Bai, Y. B. Liu, and J. Xu, "Effect of gas pressure on gas seepage of outburst coal," *Journal of China Coal Society*, vol. 35, no. 4, pp. 595–599, 2010.

[34] J. G. Ning, J. Wang, Y. L. Tan, and Q. Xu, "Mechanical mechanism of overlying strata breaking and development of fractured zone during close-distance coal seam group mining," *International Journal of Mining Science and Technology*, vol. 30, no. 2, pp. 207–215, 2020.